Effect of target shape on fast electron emission in femtosecond laser-plasma interactions

Y. T. Li,[1] M. H. Xu,[1] X. H. Yuan,[1,2] W. M. Wang,[1] M. Chen,[1] Z. Y. Zheng,[1] Z. M. Sheng,[1,3] Q. Z. Yu,[1] Y. Zhang,[1] F. Liu,[1] Z. Jin,[1] Z. H. Wang,[1] Z. Y. Wei,[1] W. Zhao,[2] and J. Zhang[1,3,*]

[1]*Beijing National Laboratory for Condensed Matter Physics, Institute of Physics, Chinese Academy of Sciences, Beijing 100080, China*

[2]*State Key Laboratory of Transient Optics Technology, Chinese Academy of Sciences, Xi'an 710068, China*

[3]*Department of Physics, Shanghai Jiao Tong University, Shanghai 200240, China*

(Received 8 June 2007; revised manuscript received 6 November 2007; published 22 January 2008)

Fast electron emission from the interaction of femtosecond laser pulses with shaped solid targets has been studied. It is found that the angular distributions of the forward fast electrons are highly dependent upon the target shapes. The important roles played by the electrostatic fields built up at the non-laser-irradiated target surfaces and the collisions in the target are identified. Our two-dimensional particle-in-cell simulations with binary collisions included reproduce the main experimental observations.

DOI: 10.1103/PhysRevE.77.016406 PACS number(s): 52.38.Kd, 52.38.−r, 52.50.Jm

I. INTRODUCTION

In the interaction of a high intensity relativistic laser pulse with a solid foil, a large number of electrons can be accelerated to very high energies, forming so-called fast electrons. Some of the fast electrons are ejected backward from the interaction region into the vacuum in front of the target. The others transport into the overdense plasma and cold target region and, finally, part of them escape from the rear target surface. Methods to control and guide the forward fast electron beam are of significance for fast ignition in inertial confined fusion [1], high-energy ion generation [2], x-ray emission [3], etc.

The guiding of fast electron beams relies on several physical processes in the target such as collisions of single electrons with atoms and other electrons, the conductivity, and self-induced electric or magnetic fields induced by the fast electrons. The collision effect will scatter the electron beams. The fast electrons tend to propagate in the high conductivity region, where the fast electron current can be compensated for by a return current of the background cold electrons. The huge fast electron current will induce strong electrostatic fields and magnetic fields in the plasma or target bulk. The bulk fields, in turn, will affect the fast electron transport. The feedback processes between the fast electrons and the bulk fields can lead to a self-organized propagation of fast electrons. First, the electrostatic fields will lead to an effective energy loss of the fast electrons and inhibit the electron penetration [4–8]. Second, the fast electron beam may be pinched by the static magnetic fields [9–12]. Finally, the fast electron beam may be broken up into filaments due to the instabilities [13,14], resulting in a self-organized state in which the net current of each filament is less than the Alfven limit [15]. Strong electric fields or magnetic fields are induced not only in the target bulk, but also at the target surfaces. The transverse electron transport and guiding at the *laser-irradiated* target surface due to the fields have been identified [16–19]. Recently methods to manipulate the fast electrons using a nonirradiated target surfaces have also attracted much attention. Preliminary simulations suggest that the collimated propagation of fast electrons through solid targets can be achieved using vacuum gaps and/or radially graded materials, which result in confining electric fields [20]. Measurements of the ultraviolet optical emission from the rear surface of an aluminum plane foil attached to a solid cylindrical or a tapered target indicates the feasibility of guiding fast electrons through a carefully shaped target. Guiding of high-density MeV electrons by a fine fiber attached to a hollow cone target has been demonstrated [21].

In this paper, we present direct observations of fast electron emission from the interaction of short laser pulses with various shaped solid targets. We find that the angular distribution of the escaped fast electrons is highly dependent on the target shape. With our two-dimensional (2D) particle-in-cell (PIC) code, KLAP, and the Monte Carlo code, ITS 3.0 (integrated TIGER series of coupled electron/photon) [22], the roles of the electrostatic fields generated at the interface between the target and the vacuum and the collisional effect in the target are identified.

II. EXPERIMENTAL SETUP

The experiments were carried out using the Xtreme Light II (XL-II) laser system at the Institute of Physics, Chinese Academy of Sciences. The laser system can produce a linearly polarized pulse with energy up to 500 mJ in a duration of 30 fs at a wavelength of 800 nm. The amplified spontaneous emission (ASE) was measured to be $\sim 10^{-5}$ of the peak intensity of the laser pulse. Figure 1 shows a schematic view of the fast electron measurement and targets used. The laser pulse was focused by an f/3.5 off-axis parabolic mirror to a focal spot size of 10–15 μm in diameter. Planar, cylindrical, and wedged copper targets were used, respectively. The standard planar target was a 65 μm thick copper disk with a diameter of 1000 μm. The cylinder had a diameter of 100 μm and length of 600 μm. The wedged target was an isosceles wedge with a tip angle of 25°, height of 150 μm

*Author to whom correspondence should be addressed. jzhang@aphy.iphy.ac.cn

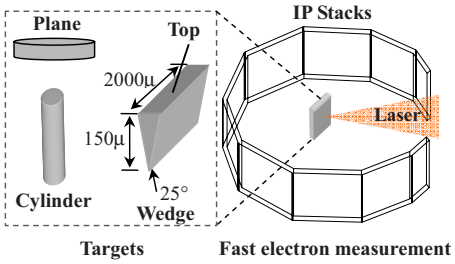

FIG. 1. (Color online) Schematic view of the shaped targets and fast electron measurement in the experiment. Planar, cylindrical, and wedged targets were used. Fast electrons were measured by IP stacks around the targets.

(from the tip to the top surface opposite the tip), and length of 2000 μm.

Utilizing the photostimulated luminescence effect, imaging plate (IP) is a new filmlike radiation image sensor comprised of specifically designed phosphors that trap and store the radiation energy. The stored energy is stable until scanned with a laser beam, which releases the energy as luminescence. Unlike the radiochromic films, the signals recorded on IP can be read out with a commercial reader electrically. IP has been developed to measure fast electrons generated from intense laser-plasma interactions, with the advantages of a high sensitivity, a large dynamic range, and good linearity compared to other conventional detectors [23]. In our experiments, spatial distributions of the forward fast electrons behind targets were measured by an array of IP stacks, which surrounded the laser focus region in the plane of laser incidence. The distance from the focus to the stacks was 55 mm. Each stack consisted of four layers of IP. The width of the IP was 50 mm. The electron energy ranges were chosen by the aluminum filters in front of the first IP layer and those inserted in adjacent layers.

III. EXPERIMENTAL RESULTS AND DICUSSSIONS

A. Identification of the effect of target shapes

First, we compare the fast electrons emitted from the wedged targets with those from the planar targets. Figures 2(a)–2(c) show the angular distributions of the forward fast electrons with energies greater than 300 keV in the laser incident plane for the planar and wedged targets, respectively. The insets illustrate the target shape and orientation. The laser pulse was incident with an angle 25° relative to the front target normal direction. The angle 0° and 90°/−90° correspond to the front target normal and the target surface, respectively. For the wedged target, the laser pulse was focused on one of the isosceles surfaces rather than the top surface opposite the tip of the wedge (see the insets in Fig. 2). The laser focus was close to the wedge tip, where the target thickness was 65 μm (which is the same as that of the planar target). The laser energy was between 60–80 mJ for the shots. For the standard planar target, the fast electron emission peaks between the laser propagation and target normal direction. This is similar to the previous observations [24]. However, for the wedged target, the peak of the fast

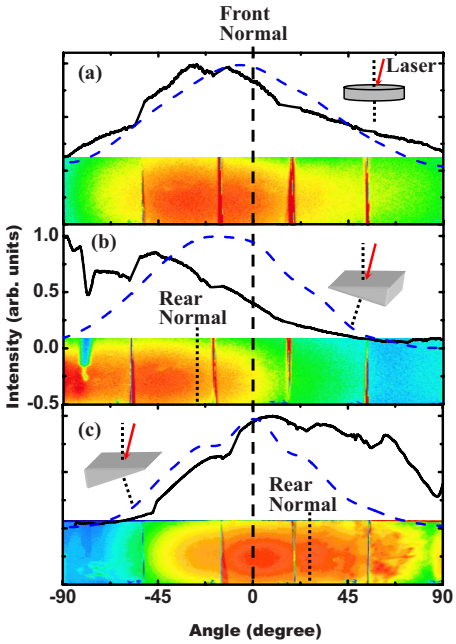

FIG. 2. (Color online) IP images of the $E>300$ keV fast electrons for a (a) planar, (b) 25° wedged, and (c) 25° wedged target rotated by 180°, respectively. One of the isosceles (side) surfaces of the wedged target was irradiated by the laser pulse. The solid lines are the scanned intensity distributions. The dashed lines are theoretical results simulated by the MC code ACCEPT. The insets illustrate the target shape and orientation.

electrons is shifted approximately towards the normal direction of the rear target surface, which is significantly deviated from the laser propagation and the front target normal direction. More interestingly, when the wedged target is rotated by 180°, the distribution is also rotated correspondingly, as shown in Fig. 2(c). One may note that the divergence angles of the fast electrons from the wedged target are also larger than that from the planar target. These results demonstrate that the target shape, especially the orientation of the rear surface, can significantly modify fast electron emission.

We have used the 3D Monte Carlo code, ACCEPT, which is one of subcodes of the ITS 3.0 system, to model the *pure collisional effect* on the fast electron transport in the cold copper targets. The ITS system permits a state-of-the-art Monte Carlo solution of linear time-integrated coupled electron-photon radiation transport problems with or without the presence of macroscopic electric and magnetic fields of arbitrary spatial dependence. The physical processes taken into account in the system include electron-positron interactions (energy loss straggling, elastic scattering, production of knock-on electrons, impact ionization followed by production of fluorescence photons and/or Auger electrons, production of bremsstrahlung, and annihilation radiation) and photon interactions (photoelectric absorption with the production of photoelectrons, Auger electrons, and fluorescence photons, incoherent scattering with the production of scattering electrons, coherent scattering, and pair production) [25]. In the MC simulations, we assumed a disk electron source with a radius of 10 μm. The energy spectrum was a Maxwellian distribution with a temperature 200 keV. The electrons were

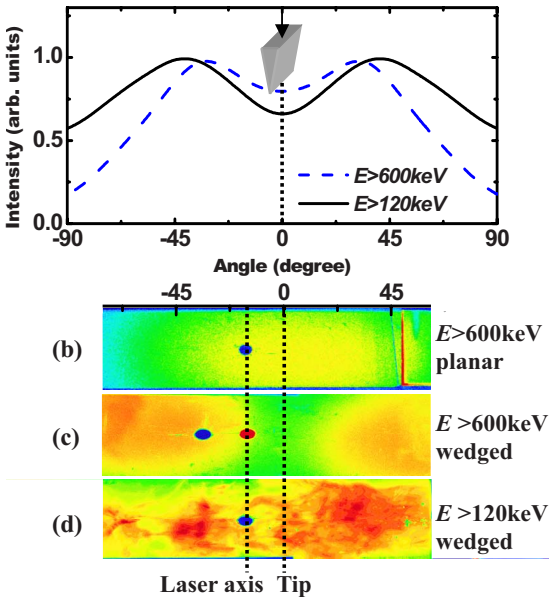

FIG. 3. (Color online) Angular distributions of the $E>600$ keV (solid) and $E>120$ keV (dashed) fast electrons simulated by (a) the MC code ACCEPT; Experimentally-measured IP images of the $E>600$ keV fast electrons from a (b) planar, (c) $E>600$ keV, and (d) $E>120$ keV fast electrons from a 25° isosceles wedged target, respectively. The top surface opposite the tip of the wedged target was irradiated by the laser pulse.

injected into the target at 25° with respect to the front target normal with a 50° cosine-law angular distribution. The distributions of the escaped electrons from the target rear surface modeled by the MC code are also shown in Fig. 2 (see the dashed lines). For comparison, all experimental and theoretical distributions are normalized. One can see, even for the $E>300$ keV electrons (which have penetration ranges that are usually considered to be much longer than the target thickness), the collisional effect still makes the electrons slightly deflected to the thin 25° tip of the wedge. However, the deflections are not large enough to reproduce the observed distributions. This indicates that the self-generated fields should play important roles in the fast electron emission besides the classical collisions. This will be further discussed in the following sections.

B. Identification of the guiding of the fast electrons

Angular distributions of the fast electrons were also measured when the laser pulse was incident from the top surface opposite the tip of the wedge. To check the pure collision effect, we first ran MC simulations in which an electron beam was normally injected into the wedge from the top. Figure 3(a) shows the simulated distributions for a $E>120$ and 600 keV electron beam. The inset shows the orientation of the target. The central part of the electron beams is depressed due to the collisions. This manifests itself as two peaks on both sides of the isosceles surfaces. The separation of the two peaks is larger, and the concavity is deeper for the low energy electrons than that for the high energy electrons.

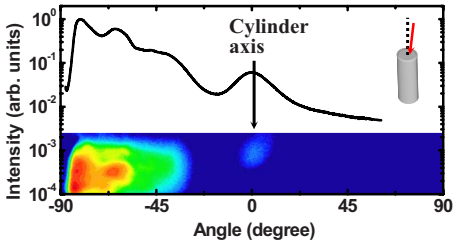

FIG. 4. (Color online) Angular distributions of the $E>300$ keV fast electrons emitted from a 600 μm long, 100 μm diameter cylindrical target. A collimated fast electron jet emitted along the cylinder axis (0°) is presented.

Figures 3(b)–3(d) show the experimentally measured angular distributions for the planar and wedged targets, the tops of which were irradiated by a laser pulse with an energy of 150–180 mJ, respectively. The laser incidence angle was 15°. The $E>600$ keV fast electrons are emitted with a single smooth peak near the target normal for the planar [see Fig. 3(b)], while with double peaks on the both sides of the isosceles surfaces for the wedged [see Fig. 3(c)]. This is similar to the profile predicted by the MC code. However, the measured distribution of the $E>120$ keV fast electrons is very different from the MC simulations. A large number of $E>120$ keV electrons are also emitted in the tip direction [see Fig. 3(d)], resulting in a distribution without an obvious concavity at the central part.

The discrepancy between the experimental measurement and the MC simulations for the low-energy fast electrons indicates there must be other effects overtaking the collision effect. We attribute this to the confinement of the electrostatic fields at the two side (rear) surfaces of the wedged target. The fields are induced when the forward fast electrons generated at the front target surface are transported to the side surfaces. It is well known that the velocity distribution of the fast electrons is Maxwellian. The fast electrons with the highest energies reach the side surfaces in advance of the moderate and low energy electrons. The induced fields are weak at the early stage because the number of such electrons is small. However, as more and more electrons reach the side surface, the fields grow rapidly. The fields have a larger effect on the moderate and low energy electrons than the high energy ones. Therefore, some moderate and low energy electrons are inhibited from escaping into vacuum and are confined in the target [note that the fields also accelerate ions by the normal sheath acceleration (TNSA) mechanism [2]]. Thus, the moderate and low energy electrons tend to be emitted towards the wedge tip (also see Fig. 6).

Note that there are some spotted structures in the IP image for the low energy electrons, while no such structures exist for the high energy electrons. This is probably caused by the instabilities of the electron transport inside the target due to the large current (number) of the low energy fast electrons [15] and/or the inhomogeneous distribution of the sheath field due to the surface quality effects of the targets, such as corrugations or nonsmooth surfaces.

Figure 4 shows the distribution of the $E>300$ keV fast electrons emitted from a 600 μm long, 100 μm diameter

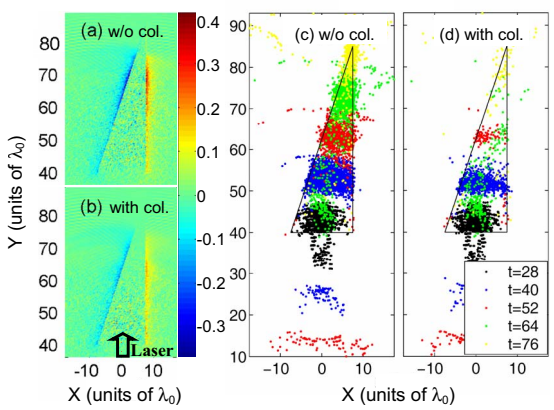

FIG. 5. (Color online) Snapshots of the electrostatic field E_x obtained by 2D PIC simulations (a) without and (b) with collisional effect at $t=60$ laser cycles; the simulated distributions of the fast electrons with relativistic factor $\gamma>4$ (c) without and (d) with collisional effect at $t=28$, 40, 52, 64, and 76 laser cycles, respectively. The laser was incident from the bottom.

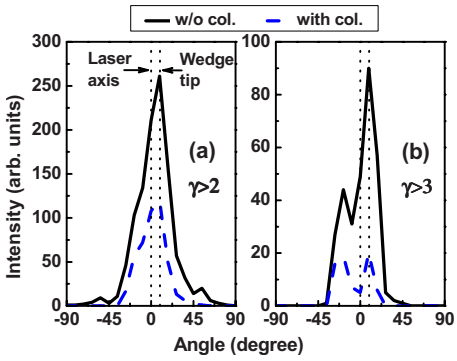

FIG. 6. (Color online) Angular distributions of the (a) $\gamma>2$ and (b) $\gamma>3$ fast electrons measured in the region $Y>87\lambda_0$ at $t=76$ laser cycles without (solid) and with (dashed) collisional effect considered in the 2D PIC simulations. The laser propagation (0°) and tip direction of the wedge (9.5°) are marked by the two dotted lines, respectively.

cylinder target, one end of which was irradiated by a 150 mJ laser pulse at a incidence angle 10°. Note that the Y-axis scale is logarithmic. Most electrons are not confined by the cylinder. However, a collimated fast electron jet emitted along the cylinder axis (0°) is presented clearly, similar to the result obtained with a hollow cone-wire target irradiated by a picosecond laser pulse with much higher energies [21]. The divergence of the jet is about 13°, coincident with the aspect ratio of the cylinder. The ratio of the integrated intensity of the $E>300$ keV electrons within the jet to the total behind the target is about 15%. This observation shows that a cylinder is better than a wedge to guide the fast electrons. This may be due to the different spatial distributions of the self-induced magnetic fields at the target side surfaces. For the cylindrical target, the radial electric fields also in addition to the azimuthal magnetic fields surrounding the target contribute to the confinement of the fast electrons [21], while, for a wedge, the magnetic fields spreading on the side surfaces may not contribute much to the confinement. Comparison of the wedge and the cylinder shows that the azimuthal magnetic fields are also very important in electron guiding.

C. PIC simulations

When a fast electron beam transports in plasmas a return current of background cold electrons, which are strongly affected by collisions, is required to maintain the electric neutrality. This can not be simulated by the pure MC code, ACCEPT. To understand how the self-generated fields and the collisions affect the fast electron transport we have carried out two kinds of PIC simulations, with and without taking the binary collisions into account, for comparison.

In our 2D PIC simulations, a right-angle wedged plasma slab with a tip angle of 18.4°, instead of an isosceles wedge (as used in the experiment), was applied (see Fig. 5). Such a nonsymmetrical target shape allows us to identify the effect of the slope of the side surfaces. The initial electron density is $6n_c$, where n_c is the critical density. A preplasma with a density profile linearly rising from 0 to $3n_c$ in the Y direction in the first $2\lambda_0$ in the front of the slab is applied. The size of the cell is $0.0125\times0.0125\lambda_0$. The Debye length is $0.0025\lambda_0$. The total number of cells and particles are 2800×10000 and 2.52×10^8, respectively. Periodic boundary conditions are applied in the X direction while absorbing boundary conditions in the Y direction. A p-polarized laser pulse with a sine-square temporal and Gaussian spatial profile is normally incident from the bottom onto the slab. The laser electric field is in the X direction. The diameter of the laser focus is $10\lambda_0$, where λ_0 is the laser wavelength. The laser duration is 18 laser cycles. The normalized vector potential, a_0, is 2.0, which corresponds to a laser intensity of 5.5×10^{18} W/cm^2.

Figures 5(a) and 5(b) show the spatial distributions of the self-generated electrostatic fields in the X direction, E_x, at 60 laser cycles obtained without and with collisional effect considered, respectively. Figures 5(c) and 5(d) show the distributions of the propagating fast electrons with relativistic factor $\gamma>4$ at different times without and with the collisional effect. One can see that no matter whether the collisions are considered or not, strong electrostatic fields are set up at the two side surfaces of the wedge. These fields effectively inhibit the electrons from escaping into vacuum, resulting in electron guiding to the tip. However, for the collisional case, the fields at the surfaces and the confinement of the electrons are weaker than those without collisional effect. When the collisions are included, the cold electrons are less able to provide enough return current, resulting in a strong electric inhibition and energy loss of the fast electrons. Therefore, the number or the current of the fast electrons reaching the side surfaces is much reduced. This leads to the reduction of the field strength and confining effect.

Figures 6(a) and 6(b) show the angular distributions of the $\gamma>2$ and $\gamma>3$ fast electrons measured in the region $Y>87\lambda_0$ (note that the tip is at $Y=85\lambda_0$) at $t=76$ laser cycles without and with collisions included, respectively. The angles 0° and 9.5° correspond to the laser propagation and the wedge tip direction, respectively. There are two main features of the distributions. First, the fast electron numbers are reduced by more than 50% due to the energy loss mainly

caused by the electric-field inhibition. Second, most $\gamma > 2$ electrons are well guided to the tip direction. However, some $\gamma > 3$ electrons cannot be confined by the electrostatic fields and escape into the vacuum region, resulting a distribution with peaks. This is particularly obvious when collisions are considered in the simulations. The collisional PIC simulations reproduce the main experimental observation shown in Fig. 3.

IV. CONCLUSIONS

We have demonstrated significant effects of target shapes on fast electron emission in the interactions of short laser pulses with matter. The collisions in the target and electrostatic fields induced at the non-laser-irradiated target surfaces are simulated by MC and PIC codes, respectively. The results show that the fields can be used to confine and guide fast electron propagation through shaped targets. When collisions are taken into account, the fast electron number reaching the rear target surfaces are decreased significantly due to the energy loss caused by the electric-field inhibition. This leads to a reduction of the confining field strength and the electron guiding effect. It is relatively difficult to confine the high energy fast electrons though low and moderate energy electrons can be effectively controlled with the induced fields. This simple technique is useful for designing targets for potential applications.

ACKNOWLEDGMENTS

The authors greatly acknowledge L. Zhang and Y. J. Tang for the target fabrication. This work was supported by the NSFC (Grants No. 10675164, 60621063, 10334110, 10575129, 10425416, and 103335020), National Basic Research Program of China (973 Program) (Grant No. 2007CB815102), and the National High-Tech ICF program.

[1] M. Tabak *et al.*, Phys. Plasmas **1**, 1621 (1994).
[2] S. Wilks *et al.*, Phys. Plasmas **8**, 542 (2001); S. Hatchett *et al.*, Phys. Plasmas **7**, 2076 (2000); M. Allen, P. K. Patel, A. MacKinnon, D. Price, S. Wilks, and E. Morse, Phys. Rev. Lett. **93**, 265004 (2004); J. Fuchs *et al.*, Phys. Rev. Lett. **94**, 045004 (2005); M. Zepf *et al.*, Phys. Rev. Lett. **90**, 064801 (2003); Y. T. Li *et al.*, Phys. Rev. E **72**, 066404 (2005) and references therein.
[3] H. Schwoerer, P. Gibbon, S. Dusterer, R. Behrens, C. Ziener, C. Reich, and R. Sauerbrey, Phys. Rev. Lett. **86**, 2317 (2001); Z. M. Sheng *et al.*, Phys. Rev. Lett. **85**, 5340 (2000); M. Chen, Z. M. Sheng, and J. Zhang, Phys. Plasmas **13**, 014504 (2006).
[4] F. Pisani *et al.*, Phys. Rev. E **62**, R5927 (2000).
[5] J. R. Davies, A. R. Bell, M. G. Haines, and S. M. Guerin, Phys. Rev. E **56**, 7193 (1997).
[6] Y. Sentoku, K. Mima, P. Kaw, and K. Nishikawa, Phys. Rev. Lett. **90**, 155001 (2003).
[7] A. R. Bell, A. P. L. Robinson, M. Sherlock, R. J. Kingham, and W. Rozmus, Plasma Phys. Controlled Fusion **48**, R37 (2006).
[8] A. J. Kemp, Y. Sentoku, T. Cowan, J. Fuchs, and H. Ruhl, Phys. Plasmas **11**, L69 (2004).
[9] A. R. Bell and R. J. Kingham, Phys. Rev. Lett. **91**, 035003 (2003).
[10] M. Tatarakis, J. R. Davies, P. Lee, P. A. Norreys, N. G. Kassapakis, F. N. Beg, A. R. Bell, M. G. Haines, and A. E. Dangor, Phys. Rev. Lett. **81**, 999 (1998).
[11] M. Borghesi, A. J. MacKinnon, A. R. Bell, G. Malka, C. Vickers, O. Willi, J. R. Davies, A. Pukhov, and J. Meyer-ter-Vehn, Phys. Rev. Lett. **83**, 4309 (1999).
[12] L. Gremillet *et al.*, Phys. Rev. Lett. **83**, 5015 (1999).
[13] M. S. Wei *et al.*, Phys. Rev. E **70**, 056412 (2004).
[14] M. Honda *et al.*, Phys. Plasmas **7**, 1302 (2000).
[15] H. Alfven, Phys. Rev. **55**, 425 (1939); D. Batani *et al.*, Phys. Rev. E **65**, 066409 (2002).
[16] T. Nakamura, S. Kato, H. Nagatomo, and K. Mima, Phys. Rev. Lett. **93**, 265002 (2004).
[17] H. Habara *et al.*, Phys. Rev. Lett. **97**, 095004 (2006).
[18] P. McKenna *et al.*, Phys. Rev. Lett. **98**, 145001 (2007).
[19] Y. T. Li *et al.*, Phys. Rev. Lett. **96**, 165003 (2006).
[20] R. B. Campbell *et al.*, Phys. Plasmas **10**, 4169 (2003).
[21] R. Kodama *et al.*, Nature (London) **423**, 1005 (2004).
[22] J. A. Halbleib *et al.*, ITS 3.0: Integrated TIGER Series of Coupled Electron/Photon Monte Carlo Transport Codes, SAND91-1634, 1992.
[23] K. A. Tanaka *et al.*, Rev. Sci. Instrum. **76**, 013507 (2005).
[24] J. Zhang, Y. T. Li, Z. M. Sheng, Z. Y. Wei, Q. L. Dong, and X. Lu, High energy density physics **1**, 61 (2005).
[25] J. A. Halbleib, R. Kensek, G. D. Valdez, S. M. Seltzer, and M. Berger, IEEE Trans. Nucl. Sci. **39**, 1025 (1992).